Resuscitation-promoting factors are required for Mycobacterium smegmatis biofilm formation

AMERICAN SOCIETY FOR MICROBIOLOGY | Applied and Environmental Microbiology®

GENETICS AND MOLECULAR BIOLOGY

Resuscitation-Promoting Factors Are Required for *Mycobacterium smegmatis* Biofilm Formation

Christopher Ealand,[a] Binayak Rimal,[b] James Chang,[b] Lethabo Mashigo,[a] Melissa Chengalroyen,[a]* Lusanda Mapela,[a] Germar Beukes,[a] Edith Machowski,[a] Sung Joon Kim,[b] Bavesh Kana[a,c]

[a]DST/NRF Centre of Excellence for Biomedical TB Research, Faculty of Health Sciences, University of the Witwatersrand, National Health Laboratory Service, Johannesburg, South Africa

[b]Department of Chemistry and Biochemistry, Baylor University, Waco, Texas, USA

[c]MRC-CAPRISA HIV-TB Pathogenesis and Treatment Research Unit, Centre for the AIDS Programme of Research in South Africa, CAPRISA, Durban, South Africa

ABSTRACT Resuscitation-promoting factors (Rpfs) have previously been shown to act as growth-stimulatory molecules via their lysozyme-like activity on peptidoglycan in the bacterial cell wall. In this study, we investigated the ability of *Mycobacterium smegmatis* strains lacking *rpf* genes to form biofilms and tested their susceptibilities to cell wall-targeting agents. *M. smegmatis* contains four distinct *rpf* homologues, namely, MSMEG_5700 (*rpfA*), MSMEG_5439 (*rpfB*), MSMEG_4640 (*rpfE2*), and MSMEG_4643 (*rpfE*). During axenic growth of the wild-type strain, all four mRNA transcripts were expressed to various degrees, but the expression of MSMEG_4643 was significantly greater during exponential growth. Similarly, all *rpf* mRNA transcripts could be detected in biofilms grown for 7, 14, and 28 days, with MSMEG_4643 expressed at the highest abundance after 7 days. In-frame unmarked deletion mutants (single and combinatorial) were generated and displayed altered colony morphologies and the inability to form typical biofilms. Moreover, any strain lacking *rpfA* and *rpfB* simultaneously exhibited increased susceptibility to rifampin, vancomycin, and SDS. Exogenous Rpf supplementation in the form of culture filtrate failed to restore biofilm formation. Liquid chromatography-mass spectrometry (LC-MS) analysis of peptidoglycan (PG) suggested a reduction in 4-3 cross-linked PG in the Δ*rpfABEE2* mutant strain. In addition, the level of PG-repeat units terminating in 1,6-anhydroMurNAc appeared to be significantly reduced in the quadruple *rpf* mutant. Collectively, our data have shown that Rpfs play an important role in biofilm formation, possibly through alterations in PG cross-linking and the production of signaling molecules.

IMPORTANCE The cell wall of pathogenic mycobacteria is composed of peptidoglycan, arabinogalactan, mycolic acids, and an outer capsule. This inherent complexity renders it resistant to many antibiotics. Consequently, its biosynthesis and remodeling during growth directly impact viability. Resuscitation-promoting factors (Rpfs), enzymes with lytic transglycosylase activity, have been associated with the revival of dormant cells and subsequent resumption of vegetative growth. *Mycobacterium smegmatis*, a soil saprophyte and close relative of the human pathogen *Mycobacterium tuberculosis*, encodes four distinct Rpfs. Herein, we assessed the relationship between Rpfs and biofilm formation, which is used as a model to study drug tolerance and bacterial signaling in mycobacteria. We demonstrated that progressive deletion of *rpf* genes hampered the development of biofilms and reduced drug tolerance. These effects were accompanied by a reduction in muropeptide production and altered peptidoglycan cross-linking. Collectively, these observations point to an important role for Rpfs in mycobacterial communication and drug tolerance.

Received 26 March 2018 **Accepted** 10 June 2018

Accepted manuscript posted online 18 June 2018

Citation Ealand C, Rimal B, Chang J, Mashigo L, Chengalroyen M, Mapela L, Beukes G, Machowski E, Kim SJ, Kana B. 2018. Resuscitation-promoting factors are required for *Mycobacterium smegmatis* biofilm formation. Appl Environ Microbiol 84:e00687-18. https://doi.org/10.1128/AEM.00687-18.

Editor Marie A. Elliot, McMaster University

Address correspondence to Bavesh Kana, Bavesh.Kana@nhls.ac.za.

* Present address: Melissa Chengalroyen, MRC/NHLS/UCT Molecular Mycobacteriology Research Unit, DST/NRF Centre of Excellence for Biomedical Tuberculosis Research, Department of Pathology, University of Cape Town, Cape Town, South Africa.

KEYWORDS resuscitation-promoting factor, peptidoglycan, biofilms, mycobacterium

The defining characteristic of any successful bacterium lies in its ability to proliferate and adapt when faced with unpredictable, potentially hostile environmental conditions. To cope with the stresses that constrain growth, bacteria have developed divergent survival strategies, including the formation of spores, a growth advantage in stationary-phase (GASP) phenotype, or metabolic quiescence (1–3). In addition, bacteria may attach to a solid surface to form a biofilm composed of a matrix of polysaccharides, proteins, and nucleic acids. Adopting this approach offers protection against exposure to antibiotics or attack from the immune system (4–6). In the case of metabolic quiescence, bacteria are able to enter a reversible state of low metabolic activity, only to resume growth once nutrient availability improves. Transitioning back to vegetative growth would therefore require resuscitation of at least one individual cell. Common features of quiescent cells may include carbon storage mechanisms, modification of the cell wall (CW) structure, increased synthesis of RNA and proteins during entry and/or exit, maintenance of membrane energy potential, and the preservation of genome integrity (1). Thus, the characterization of enzymes that modulate bacterial growth states and/or biofilm formation may identify novel drug targets. In *Micrococcus luteus*, the resuscitation-promoting factor (Rpf) was shown to act as a bacterial cytokine by increasing the culturability of dormant bacteria (7). Rpfs are muralytic enzymes implicated in remodeling the CW through cleavage of the β-1,4-glycosidic bond in peptidoglycan (PG) (8). A large body of work has previously demonstrated the role of Rpfs in virulence and resuscitation from dormancy (9). In the human pathogen *Mycobacterium tuberculosis*, which can possibly enter a quiescent state, initial studies associated the deletion of individual *rpf* genes with no significant phenotypic consequence, suggestive of functional redundancy. However, progressive *rpf* gene loss was subsequently linked to an inability to resuscitate spontaneously from a nonculturable state (1, 9, 10). Moreover, Rpfs have been shown to be important for pathogenesis in a murine model of tuberculosis (TB) infection (8). In *Mycobacterium bovis*, *rpfE* was the only gene of five that was associated with the transition from slow to fast growth *in vitro* (11). Interestingly, the *M. luteus* Rpf was able to stimulate the growth of an aged culture of *M. tuberculosis* and recovery of *M. tuberculosis* grown in murine macrophages and in Bactec cultures, indicating a conservation of the mechanism of action (12–14). In *Listeria monocytogenes*, two Rpf proteins, Lmo0186 and Lmo2522, are collectively dispensable for growth, but a double mutant displayed an extended lag phase when grown in minimal medium (15). In the Gram-positive *Lactobacillus lactis*, a positive correlation between PG breaks and biofilm-forming capacity was observed (16). An *L. lactis* strain lacking *acmA*, a PG hydrolase gene, adhered less efficiently to solid surfaces and was unable to form biofilms relative to the wild-type strain. Interestingly, these phenotypes were complemented following the addition of lysozyme (16). Rpfs have a high degree of structural similarity to lysozymes, and in this context, the role of Rpfs in biofilm formation in mycobacteria requires further study. Additional evidence of the relationship between disturbances in PG metabolism and biofilm formation is provided in *Bacillus subtilis*, where the inhibition of PG transpeptidation and transglycosylation by D-leucine and flavomycin, respectively, disrupted biofilm formation and maturation (17).

Unlike the single essential *rpf* homologue in *M. luteus*, *M. tuberculosis* contains five *rpf*-like genes (designated *rpfA* to *rpfE*). A functional hierarchy was identified within the *rpf* gene family in *M. tuberculosis*, with *rpfB* and *rpfE* ranking above *rpfD* with respect to the phenotypes assessed (9). The *M. tuberculosis* RpfB protein is structurally complex, with five distinct domains, i.e., three tandem copies of the domain of unknown function (DUF348, PF51109), a G5 domain, and a catalytic transglycosylase domain (PF06737) (see Table S1 in the supplemental material) (18, 19). The G5 domain is widely represented in the genomes of both high- and low-GC Gram-positive bacterial genomes (6). Interestingly, the G5 domain is found in the accumulation-associated protein (AAP), a

necessary component of biofilm formation in *Staphylococcus aureus* (20). Considering this, the following outstanding questions arise. (i) What are the effects of *rpf* deletion on PG structure? (ii) What are collective versus singular physiological functions of Rpfs? (iii) Do Rpfs play a role in mycobacterial biofilm formation? Last, (iv) does a loss of Rpfs affect antibiotic susceptibility? Herein, we attempt to address these questions by assessing a panel of *rpf* deletion mutants in *Mycobacterium smegmatis*, a soil saprophyte closely related to *M. tuberculosis*.

RESULTS

***M. smegmatis rpfA* and *rpfB* homologues maintain similar gene synteny relative to *M. tuberculosis* and, together with *rpfE* and *rpfE2*, are differentially expressed *in vitro*.** We first assessed the complement of *rpf* genes in *M. smegmatis* by performing a bioinformatics search for domain and synteny conservation relative to the genome of *M. tuberculosis*. Four distinct *rpf*-like genes were detected and annotated as *rpfA*, *rpfB*, *rpfE*, and *rpfE2* (18) (Fig. 1A). Biochemical studies indicate that a conserved active-site glutamate (E) is required for resuscitation/lytic transglycosylase activity (21), and this was detected, together with conserved hydrophobic domains, in all the *rpf* homologues of *M. smegmatis* (Fig. S1A). In addition, *M. smegmatis* does not contain homologues of *rpfC* and *rpfD*. Instead, it has locally duplicated the *M. tuberculosis rpfE* homologue; these two genes are adjacent to one another, and we previously termed them *rpfE* and *rpfE2* (18) (Fig. 1A and S1B). Using *in silico* analysis to identify possible differences in biological function, we noted some interesting variations. Crystal/nuclear magnetic resonance (NMR) structures of RpfB in *M. tuberculosis* ($RpfB^{Mtb}$) (21, 22), $RpfC^{Mtb}$ (23), and $RpfE^{Mtb}$ (24) have been determined and confirm that all three share the same critical amino acids and catalytic domain organization. $RpfC^{Mtb}$ retains two lysine residues at positions 26 and 33, and the variation in amino acid composition at these positions results in different charge distributions around the ligand-binding pocket for the individual Rpfs, which has been postulated to lead to substrate specificity (23). The Lys26 residue in $RpfC^{Mtb}$ is replaced with a Tyr in $RpfA^{Mtb}$, $RpfB^{Mtb}$, and $RpfE^{Mtb}$ (Fig. S1A) and with a Leu in $RpfD^{Mtb}$ (23). In contrast, the four Rpfs in *M. smegmatis* display greater variation in amino acid composition at this position, with Tyr in RpfA in *M. smegmatis* ($RpfA^{Msm}$) and $RpfE^{Msm}$, Phe in $RpfB^{Msm}$, and His in $RpfE2^{Msm}$ (Fig. S1A). There is also variation in amino composition at the position of Lys33 in $RpfC^{Mtb}$, with the exception of $RpfB^{Msm}$.

Four of the five *M. tuberculosis rpf* genes exhibited a reduction in transcript levels following reactivation *in vivo* (25). Furthermore, gene expression from early log phase through to late-stationary phase *in vitro* showed that *rpf* genes were expressed differentially, depending on growth phase (11). Similarly, we sought to establish the gene expression patterns of the *M. smegmatis rpf* homologues in liquid culture corresponding to early logarithmic (optical density at 600 nm [OD_{600}], 0.3), mid-logarithmic (OD_{600}, 0.7), and late-logarithmic (OD_{600}, 2) phase in the wild-type strain (mc^2155). Initially, *rpfA*, *rpfB*, and *rpfE2* are expressed at low levels relative to *rpfE*, which is expressed at an approximately 10-fold higher level (Fig. 1B, $P < 0.0001$). During mid-log growth, this pattern of *rpfE* expression is maintained ($P < 0.0001$), but a simultaneous increase in the expression of *rpfE2* was also observed (Fig. 1B). As the culture progressed toward stationary phase, *rpfE* transcripts were still the most abundant ($P < 0.0001$) but had dramatically decreased relative to the earlier growth phases.

Progressive deletion of *rpf* genes affects colony morphology. To further study the physiological roles of these proteins, we generated unmarked deletions in *rpfA*, *rpfB*, *rpfE*, and *rpfE2* using site-specific allelic replacement (Fig. S2). Thereafter, several combinatorial deletion mutants were constructed as follows: deletion of *rpfB* in the Δ*rpfA* mutant to generate (i) a Δ*rpfA* Δ*rpfB* (AB) double mutant. The *rpfE* and *rpfE2* genes were subsequently deleted in this background to yield (ii) a Δ*rpfA* Δ*rpfB* Δ*rpfE* (ABE) mutant and (iii) a Δ*rpfA* Δ*rpfB* Δ*rpfE2* (ABE2) mutant, respectively. In the background of Δ*rpfABE*, *rpfE2* was deleted to yield (iv) a Δ*rpfA* Δ*rpfB* Δ*rpfE* Δ*rpfE2* (ABEE2) quadruple mutant (Fig. 2A). The genotypes of all single and combinatorial mutants were con-

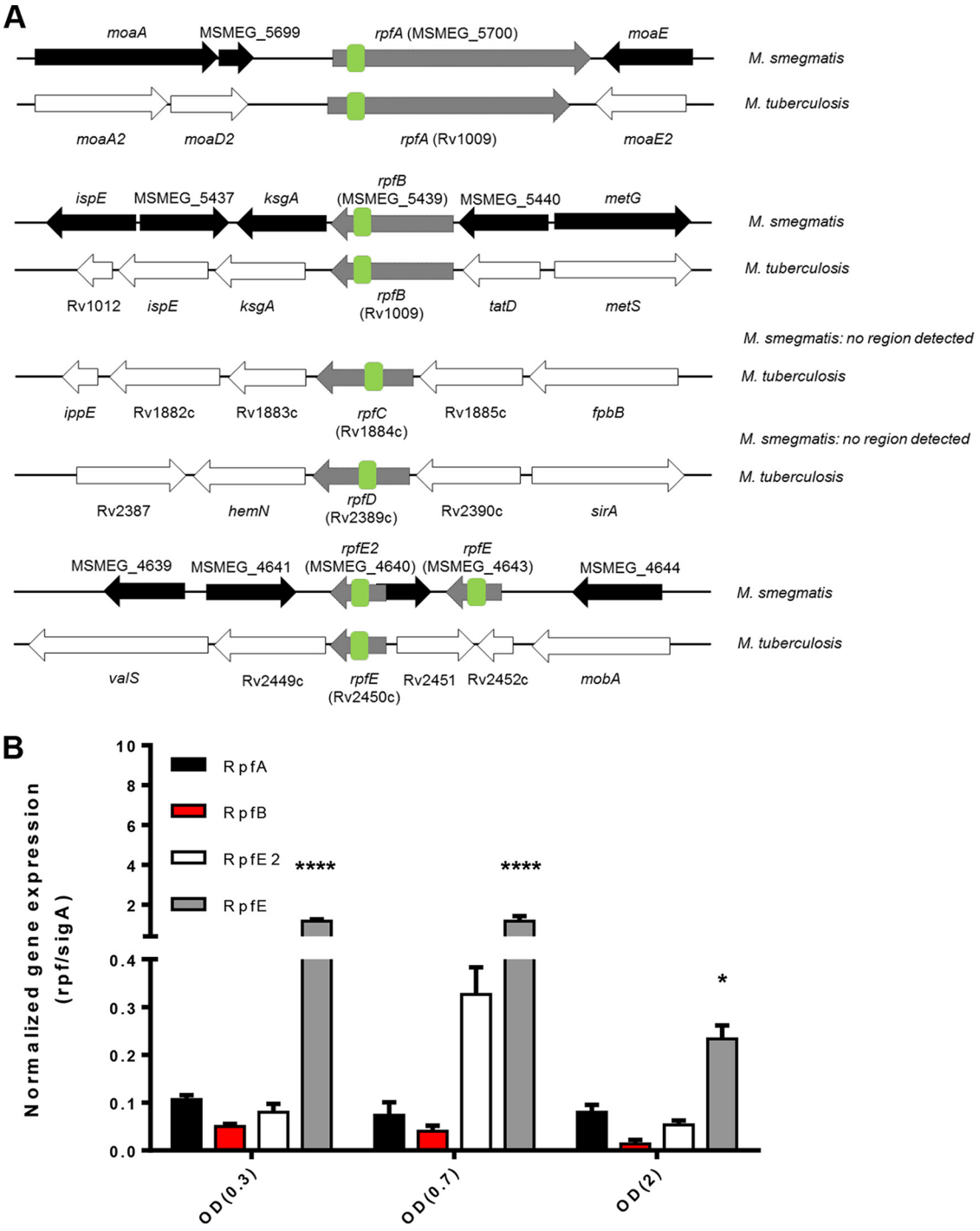

FIG 1 Schematic representation of all *M. smegmatis rpf* orthologues and their expression *in vitro*. (A) *M. smegmatis rpf* genes (gray arrows) are depicted as per their orientations in the annotated genomes (Smegmalist, black arrows [http://svitsrv8.epfl.ch/mycobrowser/smegmalist.html]) relative to the annotated genome of *M. tuberculosis* H37Rv (white arrows) (Tuberculist [http://genolist.pasteur.fr/TubercuList/index.html]). Green boxes within *rpf* genes represent the PF06737/Rpf domain. Diagram not drawn to scale. (B) Transcript levels were assessed in an axenic culture when cell densities corresponded to early logarithmic (OD_{600}, 0.3), mid-logarithmic (OD_{600}, 0.7) and late-logarithmic (OD_{600}, 2) phase. The expression of *rpf* genes was normalized against *sigA* transcript levels. Data represent the average of the results from three independent biological repeats. One-way analysis of variance (ANOVA) was used to detect statistical significance within each optical density grouping. **** and * indicate significance levels (*P* values) of <0.0001 and <0.05, respectively.

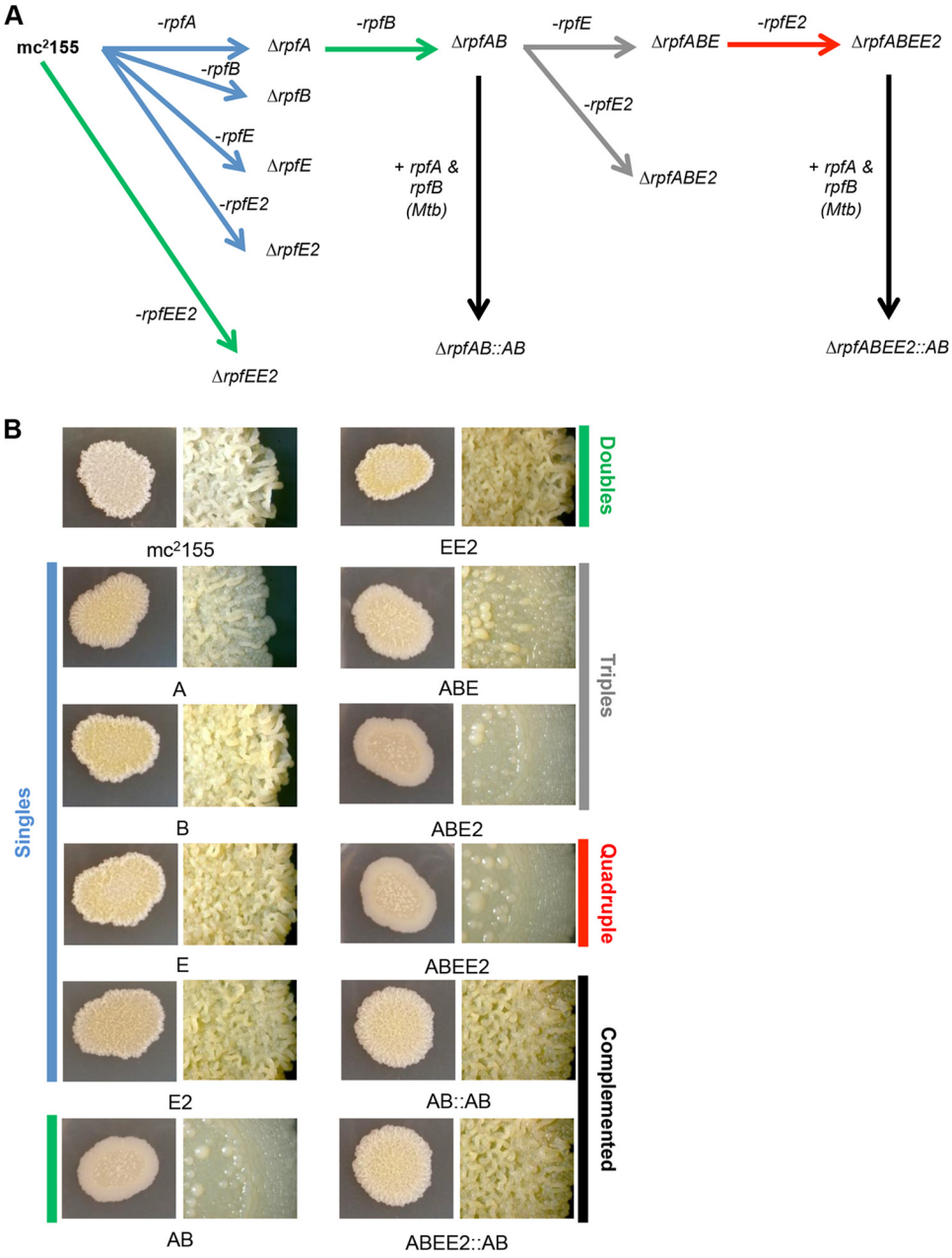

FIG 2 Construction of *rpf* deletion mutants in *M. smegmatis* and effect on colony morphology. (A) The arrows represent the stepwise in-frame deletions introduced by allelic exchange mutagenesis. Complemented strains are depicted by the black arrows. (B) Strains were grown to an optical density (OD_{600}) of 0.5, and 10 μl was spotted onto solid medium (7H10 supplemented with 1× glucose salts). Plates were incubated at 37°C for 3 to 5 days and then imaged (representative images of each strain are shown). Images on the left and right for each strain represent ×1 and ×10 magnification, respectively.

firmed by PCR and Southern blot analysis (Fig. S2A to C). Considering the close proximity of the *rpfE* and *rpfE2* genes in the *M. smegmatis* chromosome and the high sequence similarity between these two genes, we further confirmed the deletion of the *rpfE* genes in the Δ*rpfA* Δ*rpfB* Δ*rpfE* Δ*rpfE2* mutant by sequencing the deleted region (Fig. S2). When plated on solid medium, *M. smegmatis* displays substantive cording on the cell surface (26), an effect that is reduced upon the deletion of *rpf* genes. Colonies from the Δ*rpfA*, Δ*rpfB*, Δ*rpfE*, and Δ*rpfE2* single mutants displayed a marginal reduction in surface cording at the center of the colony (Fig. 2B). In the Δ*rpfAB* double-mutant strain, this loss of cording effect was exacerbated, whereas the Δ*rpfEE2* mutant strain

appeared more like the single deletions. In the Δ*rpfAB* double-mutant background, strains containing additional gene deletions, i.e., the Δ*rpfABE* and Δ*rpfABE2* triple and Δ*rpfABEE2* quadruple mutants, displayed a loss of cording that was not further exacerbated compared to the parental strain. The surfaces of the Δ*rpfAB*, Δ*rpfABE*, Δ*rpfABE2*, and Δ*rpfABEE2* mutant strains were smoother than that of the wild type and displayed atypical surface nodules that varied in size. We next attempted to genetically complement the Δ*rpfAB* and Δ*rpfABEE2* mutants by providing the *M. tuberculosis rpfA* (Rv0867c) and *rpfB* (Rv1009) genes together on a single integrating vector, pMVrpfAB, driven by the promoter region upstream of *rpfA*. We previously generated vectors that were able to genetically complement *M. tuberculosis rpf*-deficient strains (9), and given the high degree of similarity in *rpfA* and *rpfB* between these organisms, we reasoned that these plasmids, and derivatives thereof, would be proficient in heterologous complementation of the *M. smegmatis rpf* mutants. Expression analysis in the single-deletion-mutant strain, Δ*rpfB*::pMVrpfAB (B::AB), and double-deletion-mutant strain, Δ*rpfAB*::pMVrpfAB (AB::AB), revealed that both *rpfA* and *rpfB* were expressed in excess of the native levels for the *M. smegmatis* counterparts in mc^2155 (Fig. S4A). As expected, the cording phenotype was restored by complementation in both the Δ*rpfAB*::pMVrpfAB and Δ*rpfABEE2*::pMVrpfAB mutant strains.

In *M. tuberculosis*, the deletion of a single *rpf* gene resulted in compensatory expression changes with the remaining *rpf* genes (10). To assess if a similar situation prevailed in *M. smegmatis*, we next assessed gene expression in the deletion mutants. A loss of *rpf* genes in *M. smegmatis* did not lead to notable compensatory gene expression changes in the remaining *rpf* genes. However, we noted an increase in *rpfA* gene expression in the Δ*rpfB* mutant strain, but this effect was not statistically significant ($P = 0.15$) (Fig. S4B).

Loss of *rpf* genes results in aberrant biofilm formation. As complex colony architecture has been used as an analogy for biofilm formation in other bacterial species (27–29), we next investigated whether the observed phenotypes associated with *rpf* deletion were consistent in liquid biofilms. When grown to stationary phase, mycobacteria retain the ability to form floating biofilms at the liquid-air interface and assume a distinctive cording appearance (30–32). After 7 days of incubation (Fig. 3A), the deletion of *rpfA* led to a marginal reduction in biofilm formation but was comparable to that of the wild type at later time points (Fig. S5 and S6). The Δ*rpfB*, Δ*rpfE*, Δ*rpfE2*, and Δ*rpfEE2* mutant strains produced biofilms comparable to the wild-type strain at all the time points tested. In contrast, biofilms formed by the Δ*rpfAB*, Δ*rpfABE*, Δ*rpfABE2*, and Δ*rpfABEE2* mutant strains were impaired, producing small nodules on the surface after 7 days of incubation (Fig. 3A). This defect was maintained in these strains upon further incubation of the biofilms for 14 and 28 days (Fig. S5 and S6). This defect in biofilm formation was further investigated using a crystal violet assay in 24-well microtiter plates. Biofilm formation under these conditions allows for an assessment of adherence capacity (measured by staining the cells that stick to the wall of the well after the biofilm is removed) and biofilm biomass (measured by staining the entire biofilm). Analysis of biomass revealed that the Δ*rpfA* mutant and its derivatives (Δ*rpfABE*, Δ*rpfABE2*, and Δ*rpfABEE2* mutants), with the exception of the Δ*rpfAB* mutant, displayed a reduction in biofilm biomass at day 7 compared to that in the wild-type strain (Fig. 3B). However, statistical analysis indicated that this difference was not significant, and hence, we considered this a trend toward significance. In this context, it is noteworthy that genetic complementation of the Δ*rpfAB* and Δ*rpfABEE2* mutant strains with *M. tuberculosis* homologues of *rpfA* and *rpfB* resulted in biofilm biomass comparable to the wild type. Next, we assessed the ability of *rpf*-defective mutants to adhere during biofilm formation and found no difference in adherence capacity (Fig. 3C).

Considering the lack of statistically significant differences in biofilm biomass and adherence, we only considered the dramatic morphological differences in biofilms formed by some *rpf* deletion mutants to be significant and used morphology as a

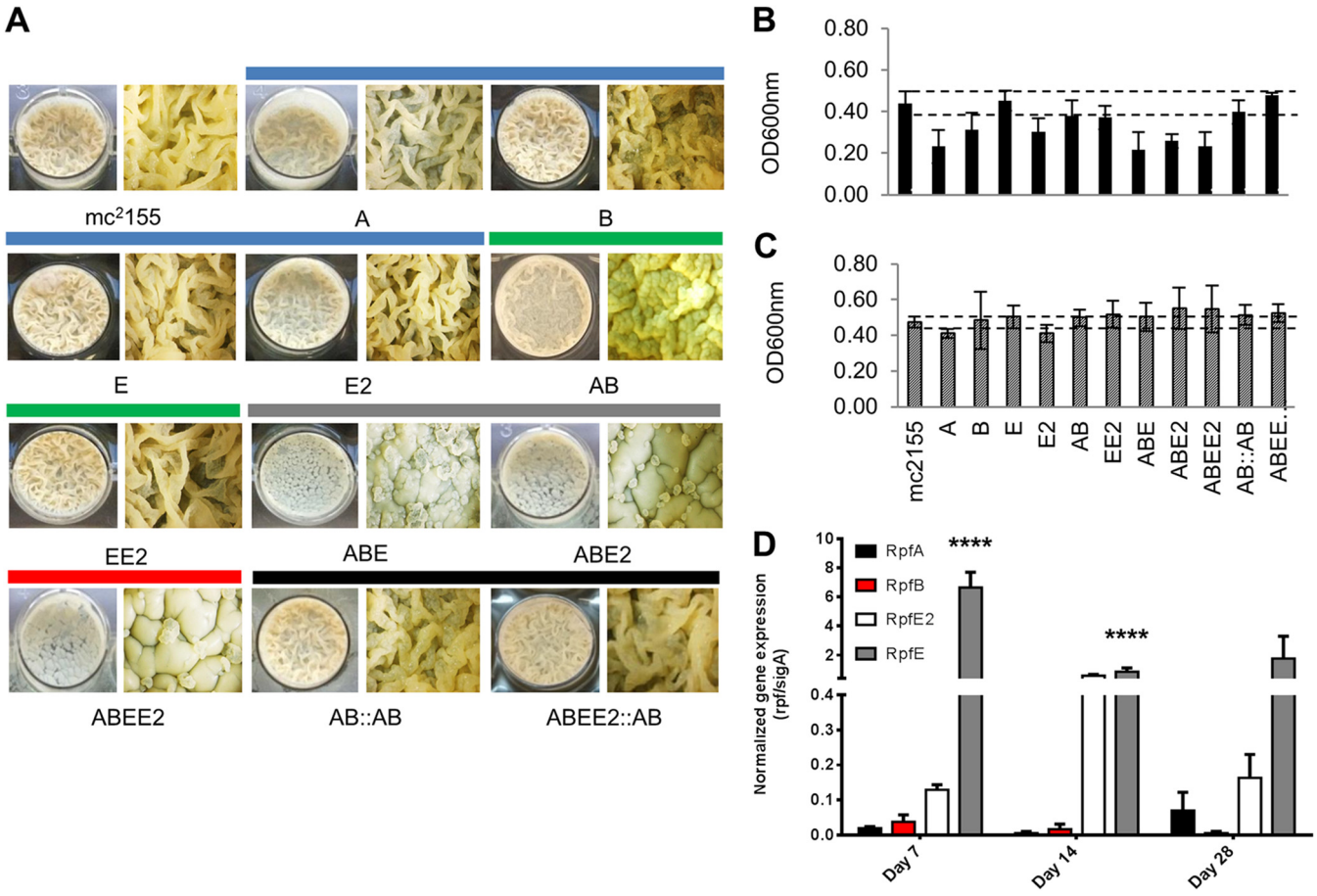

FIG 3 Characteristics of *M. smegmatis* wild-type and *rpf*-deficient biofilms. (A) Strains were adjusted to an OD_{600} of 1 and diluted 100-fold in Sauton's minimal medium (pH 7.3) in 24-well plates. Plates were sealed with Parafilm and incubated at 37°C without agitation for 7 days. Biofilms were photographed using a digital camera (×1) and a stereo microscope for greater resolution (×8 magnification). Representative images shown of three independent biological repeats. Approximately equal CFU per milliliter (data not shown) were used to start biofilms for each strain. (B) Crystal violet assay to assess biofilm biomass after 7 days. Samples were diluted 1:100, and the OD_{600} was recorded. (C) Crystal violet assay to assess biofilm adhesion after 7 days. Samples were diluted 1:10, and the OD_{600} was recorded. Absorbance measurements are representative of three independent biological repeats. Horizontal dashed lines indicate the range observed for wild type and served as a basis for interstrain comparison (no statistically significant differences were detected using a one-way ANOVA). (D) Transcript levels of *rpf* genes were assessed in wild-type biofilms at 7, 14, and 28 days. Gene expression was normalized against *sigA* transcript levels. Data represent the average of the results from three independent biological repeats. Statistical significance within each group were tested using a one-way ANOVA (**** indicates a significance level of $P < 0.0001$).

readout in subsequent experiments. In light of this, we next sought to establish the expression patterns of the *rpf* genes during biofilm formation in *M. smegmatis*. After 7 days of incubation under biofilm-inducing conditions, *rpfE* was the most highly expressed transcript. At later time points (days 14 and 28), the transcript levels of *rpfE* declined, but it was still expressed in a significant ($P < 0.0001$) excess relative to the other three genes (Fig. 3D). As *rpf* genes were differentially expressed in a wild-type biofilm, we reasoned that the observed defects in the combinatorial mutant strains were due to the absence of Rpfs in the culture media. The demonstrated secretion of Rpfs into the culture filtrate (CF) suggests that CF serves as an appropriate source of exogenous Rpf supplementation (12). To further investigate this, we assessed biofilm formation in the presence of exogenously provided culture filtrate (CF) derived from wild-type biofilms. In this case, supplementation with CF did not restore any of the biofilm-defective strains (Fig. S7).

Drug tolerance in biofilms is negatively affected following deletion of *rpf* genes. We previously demonstrated that the combinatorial loss of *rpf* genes in *M. tuberculosis* resulted in an increase in susceptibility to detergents (SDS) and antibiotics (vancomycin and erythromycin) (9, 33). Following our observations regarding defective

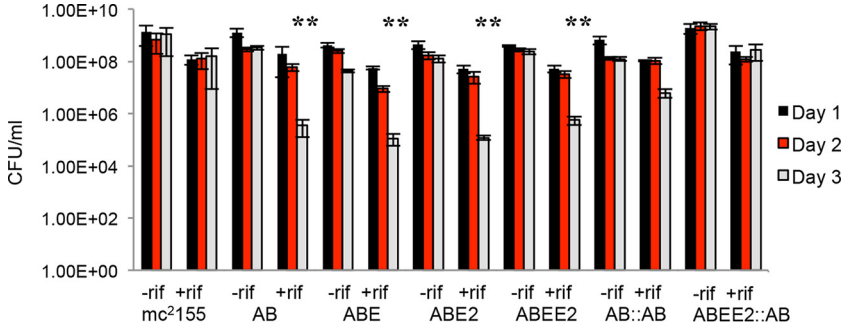

FIG 4 Rifampin tolerance of *M. smegmatis* wild-type and *rpf*-deficient strains with established biofilm defects. Strains were adjusted to an OD_{600} of 1 and diluted 100-fold in Sauton's minimal medium (pH 7.3) in 24-well plates. Plates were sealed with Parafilm and incubated at 37°C without agitation. After 7 days, wells were treated with 10× rifampin (rif), and no-drug wells served as controls. A one-way ANOVA was used to calculate statistical significance only in drug-treated samples relative to the wild type at each day (** represented $P < 0.05$ for day 3 samples). Data are representative of the results from three independent biological repeats (six repeats for mc²155).

biofilm formation in combinatorial mutants lacking *rpfA* and *rpfB*, we hypothesized that the inherent drug tolerance of these defective biofilms would be adversely affected (34, 35). To test this, we analyzed the susceptibility of the mutants with impaired biofilms to rifampin. Biofilms were exposed to a high drug concentration (ca. 10× the MIC = 312.5 μg/ml), and survival was established by calculation of CFU per milliliter relative to the untreated control at predefined time points (i.e., days 1, 2, and 3). During the first 2 days, all strains tested displayed a comparable, but insignificant, drop in viability (Fig. 4). However, after 3 days, the viabilities of the Δ*rpfAB*, Δ*rpfABE*, Δ*rpfABE2*, and Δ*rpfABEE2* mutant strains decreased significantly (approximately 100-fold) compared to that of the wild type ($P < 0.05$). To confirm that these defects were not associated with an inherent susceptibility defect, we assessed the drug sensitivities of the mutants to rifampin in broth culture. Under these conditions, the *rpf* deletion mutants displayed no increased susceptibility to rifampin (Table 1).

Rpf deletion leads to increased susceptibility to cell wall-targeting agents. We next assessed the susceptibilities of *rpf*-deficient mutants to CW-damaging agents by growing strains on solid medium supplemented with SDS (0.004%), vancomycin (3 μg/ml), erythromycin (5 μg/ml), and meropenem (1 μg/ml; Fig. 5). In agreement with MIC experiments performed in broth culture (Table 1), susceptibilities to vancomycin and SDS increased in the Δ*rpfAB*, Δ*rpfABE*, Δ*rpfABE2*, and Δ*rpfABEE2* mutant strains (Fig. 5B and C).

Cross-linking (4-3) in Δ*rpfABEE2* mutant is reduced. The PG-repeat unit in *M. smegmatis* consists of a disaccharide GlcNAc-MurNAc with a pentapeptide stem L-Ala-

TABLE 1 MICs of mycobacterial strains using various classes of antibiotics

	MIC (μg/ml)[a]								
		Single mutants		Double mutants		Triple mutant	Quadruple mutant		
Antibiotic	mc²155	Δ*rpfA*	Δ*rpfB*	Δ*rpfA* Δ*rpfB*	Δ*rpfE* Δ*rpfE2*	Δ*rpfA* Δ*rpfB* Δ*rpfE*	Δ*rpfA* Δ*rpfB* Δ*rpfE* Δ*rpfE2*	Δ*rpfA* Δ*rpfB*::pMVrpfAB	Δ*rpfA* Δ*rpfB* Δ*rpfE* Δ*rpfE2*::pMVrpfAB
Rifampin	0.625	0.625		0.625		0.625	0.625	0.625	
Vancomycin	3.125	6.25	3.125	0.781	0.781	0.39	0.39	1.562	1.562
Erythromycin	6.25	6.25	3.125	3.125	6.25	6.25	0.39	1.56	0.78
Ampicillin	18.75	75	18.75	78	78	78	150	300	600
Imipenem	20	20	0.625	0.156	0.31	0.625	0.31	1.25	0.625
Cefamandole	64	512	128	32	32	8	64	256	128
Cefapirin	100	50	25	50	12.5	25	25	25	25
Cefoxitin	80	80	40	40	20	2	2.5	80	80
Cefotaxime	100	100	6.25	25	12.5	3.125	3.125	100	100

[a]Data are representative of at least three biological replicates. Missing values indicate that tests were not performed on this strain(s).

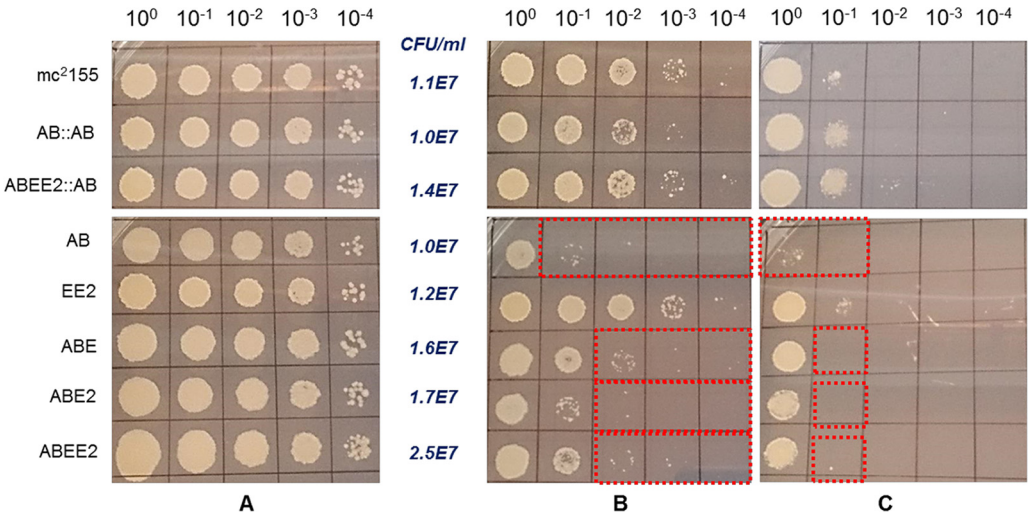

FIG 5 Drug susceptibility and permeability of the wild type, *rpf*-deficient strains, and complemented derivatives. (A to C) No-drug control (7H10 only) (A), 3 μg/ml vancomycin (B), and 0.004% SDS (C). Strains were grown to an OD_{600} of 0.4 and then serially diluted down to 10^{-6}. Ten microliters of each dilution was then aliquoted onto solid medium (7H10 supplemented with appropriate compound) and incubated at 37°C for 4 days. The starting concentration in CFU per milliliter is indicated in blue text. Red boxes highlight susceptibility differences.

D-iso-Gln-*m*-Dap-D-Ala-D-Ala attached to the lactic moiety of MurNAc (Fig. 6A). The glycan chains are cross-linked by transpeptidases that form a peptide bond between the carbonyl carbon of the *m*-Dap sidechain from an acceptor stem to the carboxyl carbon of the D-Ala at the fourth position (4-3 cross-link) or to the *m*-Dap at the third position (3-3 cross-link) in the donor stem of the neighboring glycan (Fig. 6B and C). Mutanolysin digestion of an isolated cell wall cleaves the β-1,4-glycosidic linkage of the glycan (Fig. 6A), resulting in muropeptide fragments with intact cross-links. The muropeptide ions detected by liquid chromatography-mass spectrometry (LC-MS) were identified by matching the observed *m/z* values to the corresponding entries in muropeptide library generated *in silico* using MATLAB. Each of the muropeptide fragments was accurately quantified by integrating the extracted ion chromatogram (XIC) of the identified ions (36, 37). Forty-eight muropeptide species from mc²155 and 40 species from the Δ*rpfABEE2* mutant were selected and quantified for analysis. The selected muropeptide species included the following chemical modifications to the PG-repeat unit: glycolylation, amidation, *O*-acetylation, and 1,6-anhydromuramic acid. Mutanolysin-digested isolated CW of mc²155 and the Δ*rpfABEE2* mutant primarily consisted of PG dimers, which suggest low PG cross-linking in *M. smegmatis* (38). The schematic representation of 3-3 and 4-3 cross-linked PG dimers categorized based on the total number of D-Ala found in a muropeptide is depicted in Fig. 6D. The PG dimers with 0 D-Ala and 3 D-Ala are unique to 3-3 and 4-3 cross-linked dimers, respectively; whereas a dimer with 1-2 D-Ala can be attributed to either 3-3 or 4-3 cross-linked muropeptides. Representative mass spectra of PG dimers with various chemical modifications are shown in Fig. S8 and S9. The PG dimer distributions for mc²155 and the Δ*rpfABEE2* mutant, based on the number of D-Ala (Fig. 6E), suggested that 4-3 cross-linked dimers are found in relatively low abundance (9.63% ± 2.46%) in the Δ*rpfABEE2* mutant, approximately 50% less than that with mc²155 (20% ± 2.38%). These changes are suggestive of changes in the CW composition of *M. smegmatis* associated with the deletion of all four *rpf* genes.

1,6-Anhydromuropeptides are reduced in the Δ*rpfABEE2* mutant. As lytic transglycosylases catalyze the cleavage of glycan at the β-1,4-glycosidic linkage to yield 1,6-anhydroMurNAc-terminated muropeptides (Fig. 7A), we next sought to assess the changes in the end product between mc²155 and the Δ*rpfABEE2* mutant. In the wild-type strain, approximately one out of every five PG-repeat units terminated with

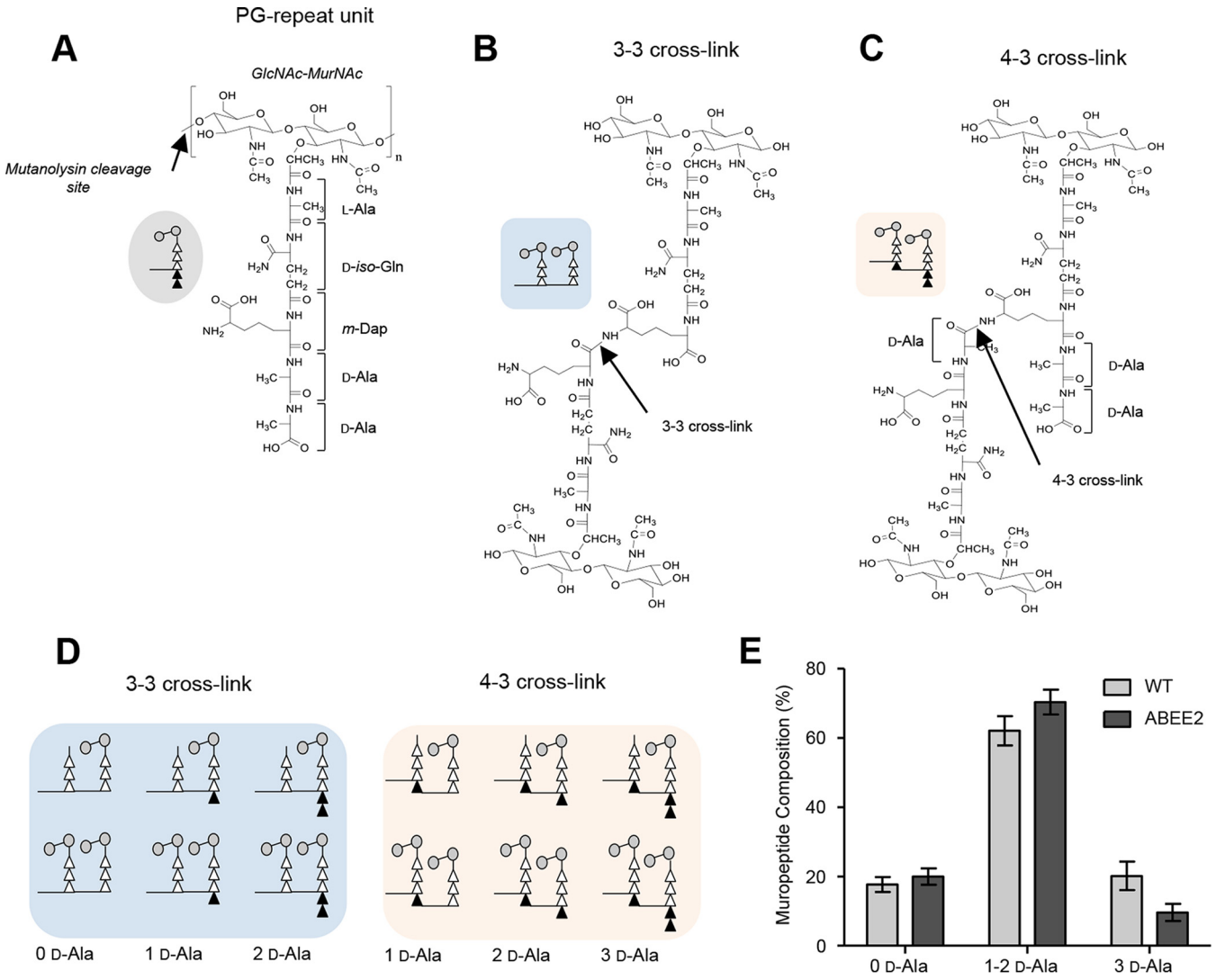

FIG 6 Peptidoglycan compositions of mc²155 and Δ*rpfABEE2* mutant strains by LC-MS. (A) Chemical structure of peptidoglycan (PG) repeat unit in *Mycobacterium smegmatis*. The PG-repeat unit consists of a disaccharide, *N*-acetylglucosamine (GlcNAc), and *N*-acetylmuramic acid (MurNAc). In *M. smegmatis*, the pentapeptide stem unit attached to the lactic moiety on MurNAc consists of L-Ala-D-iso-Gln-m-Dap-D-Ala-D-Ala. A schematic representation of a PG-repeat unit is shown as an inset, with two gray circles representing the disaccharides and five triangles to represent the pentapeptide stem. For LC-MS analysis, isolated cell walls of the mc²155 and Δ*rpfABEE2* mutant strains were digested using muramidase, which cleaves β-1,4-glycosidic linkage, indicated by an arrow. PG glycan chains are interconnected in *M. smegmatis* by 3-3 (B) or 4-3 (C) cross-links. In a 3-3 cross-link, a peptide bond is formed between the sidechain of *m*-DAP to the carbonyl carbon on the D-Ala of the neighboring tripeptide-stem structure. In a 4-3 cross-link, a peptide bond is formed between the *m*-DAP to the D-Ala of the neighboring tetrapeptide-stem structure. (D) Schematic representation of various PG dimers observed by LC-MS, with various modification probabilities in stem peptide length. The proportions of 3-3 and 4-3 cross-linked dimers are dependent on the total number of D-Ala (black triangle). (E) Composition of PG dimers found in mc²155 and Δ*rpfABEE2* mutant strains categorized based on the total number of D-Ala per muropeptide. The muropeptides without any D-Ala (0 D-Ala) consist of 3-3 cross-linked dimers, whereas the PG dimers with 3 D-Ala are unique to 4-3 cross-linked dimers. The muropeptides with 1 or 2 D-Ala can result from 3-3 or 4-3 cross-links, as shown in panel D. The muropeptide composition included all modifications, including glycolylation, amidation, *O*-acetylation, and L-amidation. In the Δ*rpfABEE2* mutant, the reduced 4-3 cross-linked PG dimers are accompanied by increased 3-3 cross-linked muropeptides. All error bars represent 95% confidence intervals ($n = 3$). The LC-MS spectra of 3-3 and 4-3 cross-linked PG dimers are shown in Fig. S8.

a 1,6-anhydroMurNAc (22.11% ± 2.54%), whereas this level decreased to one out of every eight units (12.38% ± 1.43%) in the Δ*rpfABEE2* mutant (Fig. 7B). The representative mass spectra of 1,6-anhydroMurNAc PG dimers with 1 D-Ala and 3 D-Ala are also depicted in Fig. 7C and D, respectively. The corresponding chemical structures of the 1,6-anhydroMurNAc PG dimers are shown in Fig. S9.

DISCUSSION

Bacteria encounter adverse environmental conditions and need to dynamically adapt in order to survive. The cell surface plays a major role in this adaptation, as

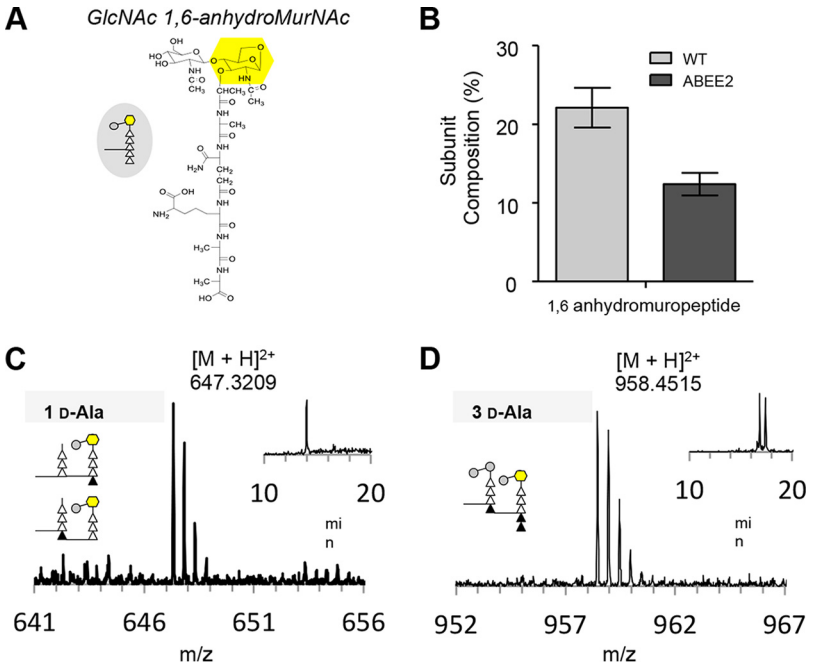

FIG 7 Peptidoglycan composition of ABEE2 mutant shows reduced concentration of the 1,6-anhydromuropeptide dimers. (A) Chemical structure of a PG monomer with a 1,6-anhydroMurNAc (yellow). Inset shows a schematic representation of a PG monomer with a 1,6-anhydroMurNAc, shown as a yellow hexagon. (B) Approximately 22.11% ± 2.54% of all PG-repeat units in mc²155 terminated in 1,6-anhydroMurNAc. In the Δ*rpfABEE2* mutant, 1,6-anhydroMurNAc-terminated muropeptides consist of 12.38% ± 1.43%, representative of an approximately 50% decrease. All error bars represent 95% confidence intervals ($n = 3$). Mass spectra of PG dimers with a 1,6-anhydroMurNAc and a PG-stem structure terminating in a tetrapeptide (C) or pentapeptide (D). Insets represent the XIC for the selected ion. The chemical structures of the 1,6-anhydroMurNAc-terminated PG dimers are shown in Fig. S9.

physical or chemical changes in composition or structure not only define particular growth states, such as sporulation, germination, and vegetative growth (39–41), but also influence bacterial signaling (42, 43). Autolysins, such as lytic transglycosylases, in combination with other PG hydrolases, play a central role via the cleavage of the glycan backbone in PG to control bacterial growth, subvert the immune response, and generate population heterogeneity (44–47). The structural similarity between Rpfs and *g*-type lysozymes (48, 49) suggests that mycobacterial Rpfs may function similarly to the lytic transglycosylases described in *E. coli* (50). However, the genetic redundancy of these genes in mycobacteria has made the study of redundant versus specialist function difficult. Furthermore, while research from several laboratories has highlighted an important role for Rpfs in virulence, growth, and survival of mycobacteria, the underlying mechanism that underpins this biological function has remained elusive. We sought to interrogate the nature of *rpf* gene function in *M. smegmatis* through combinatorial gene deletion and phenotypic assessment of the resulting mutants.

Four distinct *rpf* homologues were identified in the genome of *M. smegmatis*. Unlike *M. tuberculosis*, there is no direct $rpfD_{Mtb}$ homologue present in *M. smegmatis*; instead, there is a local duplication of *rpfE*. We also noted several amino acid changes in the Rpf catalytic domain between *M. tuberculosis* and *M. smegmatis*; however, in the case of RpfA and RpfB, our demonstrated ability to use the *M. tuberculosis* homologues to complement *M. smegmatis* mutants deficient in the corresponding homologues suggests that these differences may not materially contribute to changes in biological activity or substrate specificity.

During growth in broth, all *rpf* genes were expressed to various degrees, with *rpfE2* and *rpfE* representing the predominant transcripts, suggesting possible specialist physiological roles. In order to test this hypothesis further, we sequentially deleted each *rpf* gene to create a panel of mutants, none of which displayed any growth defects in

broth. Hence, to further probe Rpf function, we tested the ability of *rpf*-defective mutants to form biofilms, given the demonstrated role of PG hydrolases to modulate biofilm formation/maturation in other bacteria (16, 17, 51). Assessment of the transcript levels of *rpf* genes in biofilms formed by the wild type after 7, 14, and 28 days revealed that *rpfE2* and *rpfE* were highly expressed in biofilms. When testing the ability to form biofilms, single-deletion-mutant strains were indistinguishable from the wild type. In contrast, the Δ*rpfAB*, Δ*rpfABE*, Δ*rpfABE2*, and Δ*rpfABEE2* combinatorial mutants produced defective biofilms that, while able to adhere to a solid substrate, failed to mature into biofilms characteristic of the wild-type strain, even after further incubation for 14 and 28 days. These results point to a role for Rpfs in biofilm formation and possibly in maintaining the long-term stability of mycobacterial biofilms. Our results in this case are similar to those observed with the *M. smegmatis* Lsr2-defective mutant, which displayed no adhesion or substratum attachment defects but was unable to form mature biofilms, an effect that was related to GroEL1 (52). Given their high transcript abundance, it was surprising that the loss of *rpfE2* and *rpfE*, either individually or in combination, did not affect biofilm formation. The basis for this disconnect between transcript abundance and essentiality for biofilm maturation remains unclear.

In mycobacteria, biofilm formation is associated with phenotypic drug tolerance (32, 53). Our data point to a role for Rpfs in mediating this phenomenon. In all mutant strains lacking at least RpfA and RpfB, exposure to the first-line antibiotic rifampin resulted in a significant decrease in the number of cells able to tolerate high drug concentrations in biofilms. As the loss of *rpf* genes significantly attenuates the ability of *M. smegmatis* to generate mature biofilms, we propose that this reduction in phenotypic drug tolerance is related to structural defects in the biofilm rather than a change to rifampin tolerance *per se*. This is substantiated by the observation that *rpf*-defective mutants displayed no changes in susceptibility to rifampin in the broth dilution assay for drug susceptibility, which reflects growth under planktonic conditions. In contrast, changes in susceptibility to cell wall-damaging agents and detergent are most likely reflective of PG remodeling defects.

We hypothesized that exogenous supplementation of Rpfs (derived from CF isolated from the wild type) would be sufficient to restore biofilm maturation in these mutant strains. However, our results suggested that endogenous production of Rpfs is necessary for biofilm maturation and that the provision of these molecules in *trans* is insufficient to restore defects. Our experiments were limited to the use of CF, rather than recombinant Rpfs, and further work is required to test the effect of exogenous Rpf supplementation on biofilm.

The combined enzymatic actions of RpfB and RipA were previously shown to produce *N*-acetylglucosaminyl-β-1,4-*N*-glycolyl-1,6-anhydromuramyl-L-alanyl-D-isoglutamate. A synthetic 1,6-anhydrodisaccharid-dipeptide was subsequently shown to stimulate resuscitation in the dormant *M. smegmatis* model (54). This product was thus deemed the minimal structure capable of resuscitating dormant mycobacterial cells. Compositional analysis of the PG from the *rpf* quadruple mutant confirmed a reduced level of 1,6-anhydromuropeptides, thus confirming a role for Rpfs in the generation of these types of molecules.

While a large body of evidence supports the role of Rpfs as stimulatory factors in several bacterial species, their role in biofilm formation has not previously been demonstrated. Herein, we confirm that both RpfA and RpfB are required to mediate biofilm maturation and the associated phenotypic tolerance to rifampin. These findings open up new avenues to explore Rpf function in pathogenic mycobacteria.

MATERIALS AND METHODS

Bacterial strains and culture conditions. The bacterial strains and plasmid DNA constructs used in this study are listed in Tables 2 and 3, respectively. *Escherichia coli* strains were grown in Luria-Bertani (LB) or on LB agar (LA) medium. *M. smegmatis* strains were grown in standard liquid culture in Middlebrook 7H9 medium (Difco) containing 0.5% glycerol and 0.05% Tween 80 or on solid 7H10 agar medium (Difco) with 0.5% glycerol. The media were supplemented with a glucose-salt mixture to final concentrations of 0.085% NaCl and 0.2% glucose. For biofilm experiments, *M. smegmatis* strains were cultured in Sauton's medium without or supplemented with 0.05% Tween 80. Antibiotics were added to the media in final concentrations as indicated: in *E. coli*, 200 $\mu g \cdot ml^{-1}$ ampicillin, 50 $\mu g \cdot ml^{-1}$ kanamycin, or 200 $\mu g \cdot ml^{-1}$

TABLE 2 List of *Mycobacterium smegmatis* strains used and generated in this study

Strain	Description[a]	Source or reference
Escherichia coli DH5α	*supE44* Δ*lacU169* ϕ80*lacZ*ΔM15 *hsdR17 recA1 endA1 gyrA96 thi-1 relA*	Promega
M. smegmatis		
mc^{2}155	*ept-1* (efficient plasmid transformation) mutant of mc26	57
Δ*rpfA* mutant	Derivative of mc^{2}155 carrying an in-frame unmarked deletion in *rpfA*	This study
Δ*rpfB* mutant	Derivative of mc^{2}155 carrying an in-frame unmarked deletion in *rpfB*	This study
Δ*rpfE* mutant	Derivative of mc^{2}155 carrying an in-frame unmarked deletion in *rpfE2*	This study
Δ*rpfE2* mutant	Derivative of mc^{2}155 carrying an in-frame unmarked deletion in *rpfE*	This study
Δ*rpfA* Δ*rpfB* mutant	Derivative of Δ*rpfA* mutant carrying an in-frame unmarked deletion in *rpfB*	This study
Δ*rpfE* Δ*rpfE2* mutant	Derivative of mc^{2}155 carrying in-frame unmarked deletions in *rpfE* and *rpfE2*	This study
Δ*rpfA* Δ*rpfB* Δ*rpfE* mutant	Derivative of Δ*rpfA rpfB* mutant carrying an in-frame unmarked deletion in *rpfE*	This study
Δ*rpfA* Δ*rpfB* Δ*rpfE2* mutant	Derivative of Δ*rpfA rpfB* mutant carrying an in-frame unmarked deletion in *rpfE2*	This study
Δ*rpfA* Δ*rpfB* Δ*rpfE* Δ*rpfE2* mutant	Derivative of Δ*rpfA rpfB* mutant carrying in-frame unmarked deletions of *rpfE* and *rpfE2*	This study
Δ*rpfA* Δ*rpfB*::pMVrpfAB mutant	Derivative of Δ*rpfA* Δ*rpfB* mutant carrying the *Mycobacterium tuberculosis rpfA* and *rpfB* genes in pMVrpfAB integrated at the *attB* locus; Hyg^r	This study
Δ*rpfA* Δ*rpfB* Δ*rpfE* Δ*rpfE2*::pMVrpfAB mutant	Derivative of Δ*rpfA* Δ*rpfB* Δ*rpfE* Δ*rpfE2* mutant carrying the *Mycobacterium tuberculosis rpfA* and *rpfB* genes in pMVrpfAB integrated at the *attB* locus; Hyg^r	This study

[a]Hyg^r, hygromycin resistant.

hygromycin; and in *M. smegmatis*, 25 μg · ml^{-1} kanamycin or 50 μg · ml^{-1} hygromycin. Where appropriate, sucrose was added to a final concentration of 2% (wt/vol) and 5-bromo-4-chloro-3-indolyl-β-galactoside (X-Gal) to 40 μg · ml^{-1}.

Design and construction of suicide vectors for gene deletion. Suicide plasmids to introduce in-frame unmarked deletions were constructed according to the protocols outlined by Gordhan and Parish (55). Briefly, deletion alleles were generated using PCR amplicons containing the 1.2 kb upstream and downstream DNA regions for each *rpf* gene (Table 4). For the crossover strategy targeting *rpfE* and/or *rpfE2*, a different approach was taken due to the local duplication (56). The deletion allele of *rpfE* was generated from two separate fragments, whereby the central reverse-complementary primers overlapped the 5′ and 3′ triplets of the open reading frame by 15 bp each (i.e., 30 bp in total). These PCR products were purified and combined to generate template for the second PCR by acting as the sole substrate for each other at the overlapping 30 bp introduced by the PCR primer. Flanking primers were then added, and the second PCR produced the PCR product for cloning into p2NIL (Fig. S10 and Table 5) and enabled the creation of a vector that carried the deletion allele for the Δ*rpfE* and Δ*rpfE2* mutants simultaneously. The *hyg-lacZ-sacB* cassette from pGOAL19 was cloned into the unique PacI restriction sites of pNΔrpfA, pNΔrpfB, and pNΔrpfE2E to yield the delivery vectors pN19ΔrpfA, pN19ΔrpfB, and pCEM, respectively (Table 3).

Allelic exchange mutagenesis. The suicide vectors were used to transform electrocompetent *M. smegmatis* mc^{2}155 by standard methodology to generate blue (*lacZ*) single-crossover mutants resistant to kanamycin (*aph*) and sensitive to sucrose (*sacB*), according to the protocols outlined by Gordhan and Parish (55). Second-step selection in the presence of sucrose yielded white antibiotic-sensitive deletion mutant strains. Mutant alleles were distinguishable by multiplex PCR (Table 6). PCR-positive clones were further confirmed by Southern blot analysis.

Quantitative real-time PCR. In axenic cultures, strains were grown in 150 ml 7H9 broth, and samples were taken at an OD_{600} of 0.3, 0.7, and 2, followed by centrifugation at 4,000 rpm for 10 min. Bacterial cell pellets were then resuspended in 500 μl Tris-EDTA (TE) and transferred to lysing matrix B tubes (MP Biomedicals) for lysis in the MagNA lyser (Roche) at 4,500 rpm for three 40-s cycles with incubation on ice for 2 min between cycles. Three hundred fifty microliters of buffer RA1 (NucleoSpin RNA II kit; Macherey-Nagel) supplemented with 3.5 μl of β-mercaptoethanol was added to each lysed sample. The total RNA from each sample was then extracted using the NucleoSpin RNA II kit, according to the

TABLE 3 List of plasmids used and generated in this study

Plasmid	Description[a]	Reference or source
pGEM3Zf(+)	*E. coli* cloning vector, Amp^r, *lacZ*-alpha, *oriE*	Promega
p2NIL	Cloning vector; Km^r	58
pGOAL19	Plasmid carrying *hyg*, *lacZ*, and *sacB* genes as a PacI cassette; Amp^r, Hyg^r	58
pMV306	*E. coli-Mycobacterium* integrating shuttle vector	59
pMV306H	*E. coli-Mycobacterium* integrating shuttle vector; derivative of pMV306 carrying a *hyg* gene; Hyg^r	H. Boshoff
pN19ΔrpfA	Suicide vector to delete *rpfA* in *M. smegmatis*; Km^r, Hyg^r	This study
pN19ΔrpfB	Suicide vector to delete *rpfB* in *M. smegmatis*; Km^r, Hyg^r	This study
pMVrpfAB	Derivative of pMV carrying *Mycobacterium tuberculosis* H37Rv *rpfA* and *rpfB*; Hyg^r	This study
pCEM	Suicide vector to delete *rpfE* and/or *rpfE2* in *M. smegmatis*, Km^r	This study

[a]Amp^r, ampicillin resistant; Km^r, kanamycin resistant.

TABLE 4 Primers used for constructions of plasmids

Gene cloned	Primer name	Primer sequence (5′ to 3′)[a]
rpfA	rpfA-D1	GGGGGGTACCGATCTGCGGCACCTGCTG (KpnI)
	rpfA-D2	GGGGAGATCTTGGCAGATGACGAAGAAG (BglI)
	rpfA-D3	GGGGAGATCTTGGCAGATGACGAAGAAG (BglI)
	rpfA-D4	GGGGAAGCTTCCCGACGGCGACGCCGTGG (HindIII)
rpfB	rpfB-D1	GGGGAGATCTCGAAGCAACGGCGAGCGGG (BglI)
	rpfB-D2	GGGGAGATCTCGAAGCAACGGCGAGCGGG (BglI)
	rpfB-D3	GGGGAGATCTGACTATTCGACTGCTCGGG (BglI)
	rpfB-D4	GGGGAAGCTTGCGGCGCTGCGCGAAGCC (HindIII)
rpfE2 and/or *rpfE*	rpfdupF1	GCGGGGGTACCGCTAGCCCGCCTAACTAACC (KpnI)
	rpfdupR1	CTAGCCGCGCTTGCCGCACTTGCGGATGTTCTTCAC
	rpfdupF2	GTGAAGAACATCCGCAAGTGCGGCAAGCGCGGCTAG
	rpfdupR2	CTAGCGACCGAAGGCGCCCCCGAAGGCCCTCTTCAC
	rpfdupF3	GTGAAGAGGGCCTTCGGGGGCGCCTTCGGTCGCTAG
	rpfdupR3	CGGCGTCGACTCGGTCGTGGCGCGC (SalI)

[a]Underlined sequences represent restriction sites, with the restriction enzymes used shown in parentheses.

manufacturer's instructions. An on-column DNase treatment was included to remove residual genomic DNA in the RNA samples. Total RNA was quantitated on a NanoDrop spectrophotometer (Thermo Scientific), and 1 μg was further treated with Turbo DNase (Ambion, Life Technologies), according to the manufacturer's instructions. cDNA was synthesized using SuperScript III reverse transcriptase (Invitrogen, Life Technologies), according to the manufacturer's instructions. Briefly, ~23 μl of cDNA was incubated with 2 μl reverse primer mix (final concentration of 2.5 μM for each primer) using an annealing program (94°C for 1 min 30 s, 65°C for 3 min, and 57°C for 3 min) in a thermal cycler (MyCycler; Bio-Rad). Samples were then split equally, to which reverse transcriptase (RT) was either added (RT positive) or omitted (RT negative) and incubated at 50°C for 50 min, followed by inactivation at 80°C for 10 min. Quantitative real-time PCR analysis was performed on the CFX96 system (Bio-Rad), using the SsoFast EvaGreen supermix (Bio-Rad). Genomic DNA was used to generate standards in the range of 10^1 to 10^6 genomes, and transcripts were normalized against *sigA* transcript levels (Table 5). For transcript analysis in biofilms, bacterial biomass at days 7, 12 and 28 was harvested and stored in RNA*later* (Thermo Fisher Scientific) at −80°C until all samples could be processed simultaneously, as described above.

Biofilm assays. (i) Colony morphology on solid medium. Bacteria were grown to an OD_{600} of 0.5. Serial dilutions (10^0 to 10^{-6}) were prepared, and 10 μl of each dilution was aliquoted onto solid 7H10 medium. Plates were incubated at 37°C for 5 days, and colony morphology images were captured using a digital camera (Samsung Galaxy S5) and a stereo microscope for higher resolution (Zeiss Stemi 2000 microscope running on Zen 2011, blue edition).

(ii) Assessment of pellicle biofilms formed at liquid-air interface. For this biofilm model, strains were incubated in 7H9 medium supplemented with glucose salts at 37°C until they reached stationary phase. Cultures were then washed twice and adjusted to an OD_{600} of 1 in Sauton's medium (pH 7.3). Equal starting CFU per milliliter for each strain was established by plating on solid 7H10 medium, and 20

TABLE 5 Primers used for qPCR mRNA transcript analysis

Gene	Primer name	Primer sequence
sigA	Ms_sigAF	GGGCGTGATGTCCATCTCCT
	Ms_sigAR	GTATCCCGGTGCATGGTC
$rpfA_{Msm}$	Ms_rpfAF	CGTCATCTGCCAAGAACGTC
	Ms_rpfAR	GGTGTTGATCGCCCAGTTG
$rpfB_{Msm}$	Ms_rpfBF	TCGCGCAATGCGAAGCGGGTGGTA
	Ms_rpfBR	TGCCGGGATTGCGTCACCGTAGCA
$rpfE_{Msm}$	Ms_rpfEF	TGGGGTGGTGGCGCGGGT
	Ms_rpfER	AGCAGGGTCGAGCACAGC
$rpfE2_{Msm}$	Ms_rpfE2F	ACCTGGGCACCTGGCGGT
	Ms_rpfE2R	ACCGGCCAGGCGCCGATG
$rpfA_{Mtb}$	Mtb_rpfAF	CGGGTTATCGAACGCAACAC
	Mtb_rpfAR	GGTCGTTAGCGGCAAGTTCC
$rpfB_{Mtb}$	Mtb_rpfBF	TCGGATCAAGAAGGTCACCG
	Mtb_rpfBR	GCTACCGCGAACGTCACATC

TABLE 6 Primers used for genotyping *rpf*-deficient mutant strains[a]

PCR allele	Primer name	Primer sequence (5′ to 3′)	Allele, amplicon size (bp)
rpfA	rpfA_F1	GACCAGGGGCCTTTTGGC	Wild type, 1,736
	rpfA_R2	TGTCGCAGCGGACCATCG	Mutant, 395
rpfB	rpfB_F1	GTACAGGCTTAGCGAGAG	Wild type, 1,401
	rpfB_R2	CATGGTCGTGCCGATGGA	Mutant, 292
rpfE	rpfE_F1	GCGAACCCATTAGTGATC	Wild type, 771
	rpfE_R2	CGTTCGCGCGGTTCGCGA	Mutant, 407
rpfE2	rpfE2_F1	CCTTTCGTGCCTGACCGA	Wild type, 690
	rpfE2_R2	CTGCCGTACAAACGTTCA	Mutant, 386

[a]Shown for each PCR allele are a forward primer approx. 100 bp before start of deleted gene, and a reverse primer, approx. 150 bp after the stop codon of the deleted gene.

μl of each strain was added to 2 ml Sauton's medium in 24-well culture plates (Nunc), sealed with Parafilm, and incubated at 37°C for 7, 14, and 28 days. Biofilm images were captured using a digital camera (Samsung Galaxy S5) and a stereo microscope for higher resolution (Zeiss Stemi 2000 microscope running on Zen 2011, blue edition). Biofilms after 7 days were further assessed using the crystal violet assay for biomass and adhesion. After imaging, 1 ml of a 0.1% solution (prefiltered through a 0.2-μm filter) of crystal violet was added to each biofilm well and incubated at room temperature for 10 min. Planktonic bacteria and liquid media were removed by pipette, keeping the pellicle intact, and wells were allowed to dry at room temperature for 15 min. One milliliter of 95% ethanol was subsequently added, mixed by pipette, and allowed to incubate at room temperature for 15 min. The contents of each well were briefly mixed and then diluted 100-fold in 95% ethanol before measuring the absorbance at 600 nm (Spekol 1500; Analytik Jena). Adhesion was measured using the protocol outlined above, with modifications: at the selected time points, plates were tipped upside-down to remove the floating pellicle as well as the planktonic cells and media before the addition of crystal violet. The contents of each well were briefly mixed and then diluted 10-fold in 95% ethanol before absorbance measurements were made.

(iii) Drug tolerance assays. Strains defective for proper biofilm formation were grown for 7 days, as described above. Rifampin was added by pipetting onto the surface of the biofilm to three independent wells at a concentration of 312.5 μg/ml (10$\times$ the MIC), and three different wells served as a no-drug control. Plates were sealed and further incubated at 37°C. At days 1, 2, and 3, the effect of drug treatment on viability was assessed by establishing the CFU per milliliter for comparison to the no-drug controls for the same time point.

Culture filtrate supplementation. Select strains were grown in 100 ml Sauton's minimal medium (pH 7.3) until stationary phase. Cultures were centrifuged at 4,000 rpm for 10 min, and bacterial pellets were discarded. Supernatants were sterilized using a 0.22-μm filter and were subsequently split into two equal volumes. One half was diluted 1:1 with fresh Sauton's medium, while the other half was heat treated at 65°C for 30 min and then diluted similarly. These culture filtrate supernatants served as media for strains previously shown to be defective in biofilm formation to assess if (i) exogenously supplied Rpf could restore biofilm formation and (ii) the enzymatic function of Rpf could be negated via heat inactivation. Biofilms were incubated and subsequently imaged as described above.

Cell wall isolation and digestion for LC-MS. Cultures of mc^{2}155 and the Δ*rpfABEE2* mutant grown in 7H9 broth (supplemented with albumin-dextrose-catalase [ADC], Tween, and glycerol) at 37°C with 150 rpm orbital shaking were used to inoculate flasks containing 100 ml of supplemented 7H9 broth (1% [vol/vol]). Bacteria were harvested at stationary phase (OD_{600}, 1.6) by centrifugation at 4,750 rpm (Allegra X-15R with SX4750 rotor; Beckman Coulter) for 10 min. Pellets were resuspended in phosphate-buffered saline (PBS) and sterilized by immersing in a boiling water bath for 30 min. Samples were lysed by bead beating (Bead Mill 24; Fisher Scientific) with 0.5-mm-diameter glass beads for eight 1-min cycles with 1-min breaks between agitations. Beads and other contaminants were removed using a Steriflip 20-μm nylon vacuum filter (EMD Millipore). Crude cell wall pellets were resuspended in 2 ml PBS, to which 8 ml of 2% sodium dodecyl sulfate (SDS) solution was added and boiled for 30 min. Boiled cell wall pellets were washed with deionized water to remove SDS and then resuspended in 2 ml of 50 mM Tris (pH 8.0) buffer. DNase (200 μg) was added to the cell wall suspension and incubated at 37°C for 24 h with shaking (150 rpm), followed by the addition of pronase E (200 μg) for an additional 24 h of incubation. The cell walls were washed once and resuspended in 1 ml of Tris buffer. Isolated cell walls were digested by the addition of 0.5 kU of mutanolysin (Sigma-Aldrich) to the cell wall suspension at room temperature and incubated for 24 h. An additional 0.5 kU of mutanolysin was added to the mixture and further incubated for 24 h. The digested cell walls were frozen, lyophilized (Labconco), and then dissolved in 1 ml of 0.375 M sodium borate buffer (pH 9.0) using high-performance liquid chromatography (HPLC)-grade water. Muropeptides were reduced by the addition of 10 mg of sodium borohydride (Fisher Scientific) at room temperature for 30 min. The reduction was quenched by the addition of 125 μl of phosphoric acid. The reduced samples were frozen at −80°C and then lyophilized. Prior to LC-MS analysis, lyophilized samples were resuspended in 1 ml of sample preparation buffer (1% trifluoroacetic acid), centrifuge filtered, and purified for LC-MS using 100-μl Pierce C_{18} tips (Thermo Scientific).

Liquid chromatography-mass spectrometry. Mutanolysin-digested muropeptide fragments were chromatographically separated using the nanoACQUITY Ultra Performance LC system (Waters). A reverse-phase BEH C_{18} column (length, 100 mm; diameter, 75 μm) of a 1.7-μm bead with a pore size of 130 Å was used. Chromatographic separation of mutanolysin-digested PG was performed by injecting 1 μl of the sample from a 5-μl sample loop to the column under isocratic conditions of 99% buffer A (99.8% anhydrous methanol with 0.1% formic acid) and 1% buffer B (100% acetonitrile) for 5 min, and then a linear gradient to 50% buffer B was applied for 30 min for the separation. The column was regenerated under isocratic conditions with 85% buffer B for 5 min, a linear gradient to 98% buffer A for 1 min, and then isocratic conditions at 98% buffer A for 23 min. The flow rate was kept constant (0.6 μl/min) throughout the analysis. Fibrinopeptide B (Glu-Fib) was used as an internal standard to correct for drift of the instrument. Data were analyzed using MassLynx (Waters) and MATLAB (MathWorks).

SUPPLEMENTAL MATERIAL

Supplemental material for this article may be found at https://doi.org/10.1128/AEM.00687-18.

SUPPLEMENTAL FILE 1, PDF file, 1.3 MB.

ACKNOWLEDGMENTS

This work was supported by funding from an International Early Career Scientist Award from the Howard Hughes Medical Institute (to B. Kana), the South African National Research Foundation (to B. Kana and C. Ealand); the South African Medical Research Council (to B. Kana); the Centre for Aids Prevention Research in South Africa (CAPRISA, to C. Ealand and M. Chengalroyen). C. Ealand was supported by a Career Development Award from the South African Medical Research Council. We acknowledge the Baylor University Mass Spectrometry Centre (BU-MSC) for support and the National Institutes of Health through grant GM116130.

We thank Moagi Shaku for insightful comments and critical assessment of the manuscript.

C. Ealand and B. Kana designed experiments. C. Ealand, L. Mashigo, and M. Chengalroyen performed the experiments. C. Ealand, M. Chengalroyen, and B. Kana analyzed data. S. J. Kim, J. Chang, and B. Rimal conducted LC-MS and data analysis. L. Mapela, G. Beukes, and E. Machowski created the plasmid constructs and deletion mutant strains. C. Ealand and B. Kana wrote the paper.

We declare no conflicts of interest.

REFERENCES

1. Rittershaus E, Baek S-H, Sassetti C. 2013. The normalcy of dormancy: common themes in microbial quiescence. Cell Host Microbe 13:643–651. https://doi.org/10.1016/j.chom.2013.05.012.
2. Liang X, Zhu J, Zhao Z, Zheng F, Zhang E, Wei J, Ji Y, Ji Y. 2017. A single nucleotide polymorphism is involved in regulation of growth and spore formation of *Bacillus anthracis* Pasteur II strain. Front Cell Infect Microbiol 7:270. https://doi.org/10.3389/fcimb.2017.00270.
3. Stewart GC. 2017. Assembly of the outermost spore layer: pieces of the puzzle are coming together. Mol Microbiol 104:535–538. https://doi.org/10.1111/mmi.13651.
4. O'Toole G, Kaplan HB, Kolter R. 2000. Biofilm formation as microbial development. Annu Rev Microbiol 54:49–79. https://doi.org/10.1146/annurev.micro.54.1.49.
5. Sauer K. 2003. The genomics and proteomics of biofilm formation. Genome Biol 6:219. https://doi.org/10.1186/gb-2003-4-6-219.
6. Bateman A, Holden MT, Yeats C. 2005. The G5 domain: a potential *N*-acetylglucosamine recognition domain involved in biofilm formation. Bioinformatics 21:1301–1303. https://doi.org/10.1093/bioinformatics/bti206.
7. Mukamolova G, Kaprelyants A, Young D, Young M, Kell D. 1998. A bacterial cytokine. Proc Natl Acad Sci U S A 95:8916–8921.
8. Kana BD, Mizrahi V. 2010. Resuscitation-promoting factors as lytic enzymes for bacterial growth and signaling. FEMS Immunol Med Microbiol 58:39–50. https://doi.org/10.1111/j.1574-695X.2009.00606.x.
9. Kana BD, Gordhan BG, Downing KJ, Sung N, Vostroktunova G, Machowski EE, Tsenova L, Young M, Kaprelyants A, Kaplan G, Mizrahi V. 2008. The resuscitation-promoting factors of *Mycobacterium tuberculosis* are required for virulence and resuscitation from dormancy but are collectively dispensable for growth *in vitro*. Mol Microbiol 67:672–684. https://doi.org/10.1111/j.1365-2958.2007.06078.x.
10. Downing KJ, Mischenko VV, Shleeva MO, Young DI, Young M, Kaprelyants AS, Apt AS, Mizrahi V. 2005. Mutants of *Mycobacterium tuberculosis* lacking three of the five *rpf*-like genes are defective for growth *in vivo* and for resuscitation *in vitro*. Infect Immun 73:3038–3043. https://doi.org/10.1128/IAI.73.5.3038-3043.2005.
11. Tufariello JM, Jacobs WR, Jr, Chan J. 2004. Individual *Mycobacterium tuberculosis* resuscitation-promoting factor homologues are dispensable for growth *in vitro* and *in vivo*. Infect Immun 72:515–526. https://doi.org/10.1128/IAI.72.1.515-526.2004.
12. Shleeva MO, Bagramyan K, Telkov MV, Mukamolova GV, Young M, Kell DB, Kaprelyants AS. 2002. Formation and resuscitation of "non-culturable" cells of *Rhodococcus rhodochrous* and *Mycobacterium tuberculosis* in prolonged stationary phase. Microbiology 148:1581–1591. https://doi.org/10.1099/00221287-148-5-1581.
13. Biketov S, Mukamolova GV, Potapov V, Gilenkov E, Vostroknutova G, Kell DB, Young M, Kaprelyants AS. 2000. Culturability of *Mycobacterium tuberculosis* cells isolated from murine macrophages: a bacterial growth factor promotes recovery. FEMS Immunol Med Microbiol 29:233–240. https://doi.org/10.1111/j.1574-695X.2000.tb01528.x.
14. Wu X, Yang Y, Han Y, Zhang J, Liang Y, Li H, Li B, Wang L. 2008. Effect of recombinant Rv1009 protein on promoting the growth of *Mycobacterium tuberculosis*. J Appl Microbiol 105:1121–1127. https://doi.org/10.1111/j.1365-2672.2008.03850.x.
15. Pinto D, Sao-Jose C, Santos MA, Chambel L. 2013. Characterization of two resuscitation promoting factors of *Listeria monocytogenes*. Microbiology 159:1390–1401. https://doi.org/10.1099/mic.0.067850-0.

16. Mercier C, Durrieu C, Briandet R, Domakova E, Tremblay J, Buist G, Kulakauskas S. 2002. Positive role of peptidoglycan breaks in lactococcal biofilm formation. Mol Microbiol 46:235–243. https://doi.org/10.1046/j.1365-2958.2002.03160.x.
17. Bucher T, Oppenheimer-Shaanan Y, Savidor A, Bloom-Ackermann Z, Kolodkin-Gal I. 2015. Disturbance of the bacterial ell wall specifically interferes with biofilm formation. Environ Microbiol Rep 7:990–1004. https://doi.org/10.1111/1758-2229.12346.
18. Machowski EE, Senzani S, Ealand C, Kana BD. 2014. Comparative genomics for mycobacterial peptidoglycan remodelling enzymes reveals extensive genetic multiplicity. BMC Microbiol 14:75. https://doi.org/10.1186/1471-2180-14-75.
19. Ruggiero A, Squeglia F, Romano M, Vitagliano L, De Simone A, Berisio R. 2017. Structure and dynamics of the multi-domain resuscitation promoting factor RpfB from *Mycobacterium tuberculosis*. J Biomol Struct Dyn 35:1322–1330. https://doi.org/10.1080/07391102.2016.1182947.
20. Schaeffer CR, Woods KM, Longo GM, Kiedrowski MR, Paharik AE, Büttner H, Christner M, Boissy RJ, Horswill AR, Rohde H, Fey PD. 2015. Accumulation-associated protein enhances *Staphylococcus epidermidis* biofilm formation under dynamic conditions and is required for infection in a rat catheter model. Infect Immun 83:214–226. https://doi.org/10.1128/IAI.02177-14.
21. Cohen-Gonsaud M, Barthe P, Bagnéris C, Henderson B, Ward J, Roumestand C, Keep NH. 2005. The structure of a resuscitation-promoting factor domain from *Mycobacterium tuberculosis* shows homology to lysozymes. Nat Struct Mol Biol 12:270–273. https://doi.org/10.1038/nsmb905.
22. Cohen-Gonsaud M, Keep N, Davies A, Ward J, Henderson B, Labesse G. 2004. Resuscitation-promoting factors possess a lysozyme-like domain. Trends Biochem Sci 29:7–10. https://doi.org/10.1016/j.tibs.2003.10.009.
23. Chauviac F-X, Robertson G, Quay DHX, Bagneris C, Dumas C, Henderson B, Ward J, Keep NH, Cohen-Gonsaud M. 2014. The RpfC (Rv1884) atomic structure shows high structural conservation within the resuscitation-promoting factor catalytic domain. Acta Crystallogr F Struct Biol Commun 70:1022–1026. https://doi.org/10.1107/S2053230X1401317X.
24. Mavrici D, Prigozhin D, Alber T. 2014. *Mycobacterium tuberculosis* RpfE crystal structure reveals a positively charged catalytic cleft. Protein Sci 23:481–487. https://doi.org/10.1002/pro.2431.
25. Tufariello JM, Mi K, Xu J, Manabe YC, Kesavan AK, Drumm J, Tanaka K, Jacobs WR, Jr, Chan J. 2006. Deletion of the *Mycobacterium tuberculosis* resuscitation-promoting factor Rv1009 gene results in delayed reactivation from chronic tuberculosis. Infect Immun 74:2985–2995. https://doi.org/10.1128/IAI.74.5.2985-2995.2006.
26. Glickman MS, Cox JS, Jacobs WR, Jr. 2000. A novel mycolic acid cyclopropane synthetase is required for cording, persistence, and virulence of *Mycobacterium tuberculosis*. Mol Cell 5:717–727. https://doi.org/10.1016/S1097-2765(00)80250-6.
27. Branda SS, Gonzalez-Pastor JE, Dervyn E, Ehrlich SD, Losick R, Kolter R. 2004. Genes involved in formation of structured multicellular communities by *Bacillus subtilis*. J Bacteriol 186:3970–3979. https://doi.org/10.1128/JB.186.12.3970-3979.2004.
28. Morikawa M, Kagihiro S, Haruki M, Takano K, Branda S, Kolter R, Kanaya S. 2006. Biofilm formation by a *Bacillus subtilis* strain that produces γ-polyglutamate. Microbiology 152:2801–2807. https://doi.org/10.1099/mic.0.29060-0.
29. Chu F, Kearns DB, Branda SS, Kolter R, Losick R. 2006. Targets of the master regulator of biofilm formation in *Bacillus subtilis*. Mol Microbiol 59:1216–1228. https://doi.org/10.1111/j.1365-2958.2005.05019.x.
30. Kulka K, Hatfull G, Ojha AK. 2012. Growth of *Mycobacterium tuberculosis* biofilms. J Vis Exp 60:3820. https://doi.org/10.3791/3820.
31. Ojha AK, Jacobs WR, Jr, Hatfull GF. 2015. Genetic dissection of mycobacterial biofilms. Methods Mol Biol 1285:215–226. https://doi.org/10.1007/978-1-4939-2450-9_12.
32. Ojha AK, Baughn AD, Sambandan D, Hsu T, Trivelli X, Guerardel Y, Alahari A, Kremer L, Jacobs WR, Jr, Hatfull GF. 2008. Growth of *Mycobacterium tuberculosis* biofilms containing free mycolic acids and harbouring drug-tolerant bacteria. Mol Microbiol 69:164–174. https://doi.org/10.1111/j.1365-2958.2008.06274.x.
33. Kana BD, Mizrahi V. 2010. Resuscitation promoting factors in bacterial population dynamics during TB infection. Drug Discov Today Dis Mech 7:e13–e18. https://doi.org/10.1016/j.ddmec.2010.08.003.
34. Stewart PS. 2015. Antimicrobial tolerance in biofilms, p 269–285. *In* Ghannoum M, Parsek M, Whiteley M, Mukherjee PK (ed), Microbial biofilms, 2nd ed. American Society for Microbiology, Washington, DC.
35. Lewis K. 2008. Multidrug tolerance of biofilms and persister cells. Curr Top Microbiol Immunol 322:107–131.
36. Chang J, Foster E, Yang H, Kim S. 2017. Quantification of the D-Ala-D-Lac-terminated peptidoglycan structure in vancomycin-resistant *Enterococcus faecalis* using a combined solid-state nuclear magnetic resonance and mass spectrometry analysis. Biochemistry 56:612. https://doi.org/10.1021/acs.biochem.6b00774.
37. Chang JD, Foster EE, Wallace AG, Kim SJ. 2017. Peptidoglycan *O*-acetylation increases in response to vancomycin treatment in vancomycin-resistant *Enterococcus faecalis*. Sci Rep 7:46500. https://doi.org/10.1038/srep46500.
38. Senzani S, Li D, Bhaskar A, Ealand C, Chang J, Rimal B, Liu C, Kim SJ, Dhar N, Kana B. 2017. An Amidase_3 domain-containing *N*-acetylmuramyl-L-alanine amidase is required for mycobacterial cell division. Sci Rep 7:1140. https://doi.org/10.1038/s41598-017-01184-7.
39. Dworkin J, Shah I. 2010. Exit from dormancy in microbial organisms. Nat Rev Microbiol 8:890–896. https://doi.org/10.1038/nrmicro2453.
40. Meyer P, Gutierrez J, Pogliano K, Dworkin J. 2010. Cell wall synthesis is necessary for membrane dynamics during sporulation of *Bacillus subtilis*. Mol Microbiol 76:956–970. https://doi.org/10.1111/j.1365-2958.2010.07155.x.
41. Higgins D, Dworkin J. 2012. Recent progress in *Bacillus subtilis* sporulation. FEMS Microbiol Rev 36:131–148. https://doi.org/10.1111/j.1574-6976.2011.00310.x.
42. Takeuchi O, Hoshino K, Kawai T, Sanjo H, Takada H, Ogawa T, Takeda K, Akira S. 1999. Differential roles of TLR2 and TLR4 in recognition of Gram-negative and Gram-positive bacterial cell wall components. Immunity 11:443–451. https://doi.org/10.1016/S1074-7613(00)80119-3.
43. Takeuchi O, Takeda K, Hoshino K, Adachi O, Ogawa T, Akira S. 2000. Cellular responses to bacterial cell wall components are mediated through MyD88-dependent signaling cascades. Int Immunol 12:113–117. https://doi.org/10.1093/intimm/12.1.113.
44. Schokman GD, Daneo-Moore L, Kariyama R, Massiddam O. 1996. Bacterial walls, peptidoglycan hydrolases, autolysins and autolysis. Microb Drug Resist 2:95–98. https://doi.org/10.1089/mdr.1996.2.95.
45. Chen R, Guttenplan SB, Blair KM, Kearns DB. 2009. Role of the sigmaD-dependent autolysins in *Bacillus subtilis* population heterogeneity. J Bacteriol 191:5775–5784. https://doi.org/10.1128/JB.00521-09.
46. Moyniham PJ, Clarke AJ. 2011. *O*-Acetylated peptidoglycan: controlling the activity of bacterial autolysins and lytic enzymes of innate immune systems. Int J Biochem Cell Biol 43:1655–1659. https://doi.org/10.1016/j.biocel.2011.08.007.
47. Atilano ML, Pereira PM, Vaz F, Cataloa MJ, Reed P, Grilo IR, Sobral RG, Ligoxygakis P, Pinho MG, Filipe SR. 2014. Bacterial autolysins trim cell surface peptidoglycan to prevent detection by the *Drosophila* innate immune system. Elife 3:e02277. https://doi.org/10.7554/eLife.02277.
48. Squeglia F, Romano M, Ruggiero A, Vitagliano L, De Simone A, Berisio R. 2013. Carbohydrate recognition by RpfB from *Mycobacterium tuberculosis* unveiled by crystallographic and molecular dynamics analyses. Biophys J 104:2530–2539. https://doi.org/10.1016/j.bpj.2013.04.040.
49. Ruggiero A, Tizzano B, Pedone E, Wilmanns M, Berisio R. 2009. Crystal structure of the resuscitation-promoting factor (DeltaDUF)RpfB from *M. tuberculosis*. J Mol Biol 385:153–162. https://doi.org/10.1016/j.jmb.2008.10.042.
50. Scheurwater E, Reid CW, Clarke AJ. 2008. Lytic transglycosylases: bacterial space-making autolysins. Int J Biochem Cell Biol 40:586–591. https://doi.org/10.1016/j.biocel.2007.03.018.
51. Marti S, Puig C, Merlos A, Viñas M, de Jonge MI, Liñares J, Ardanuy C, Langereis JD. 2017. Bacterial lysis through interference with peptidoglycan synthesis increases biofilm formation by nontypeable *Haemophilus influenzae*. mSphere 2:e00329-16. https://doi.org/10.1128/mSphere.00329-16.
52. Yang Y, Thomas J, Li Y, Vilcheze C, Derbyshire KM, Jacobs WR, Jr, Ojha A. 2017. Defining a temporal order of genetic requirements for development of mycobacterial biofilms. Mol Microbiol 105:794–809. https://doi.org/10.1111/mmi.13734.
53. Islam MS, Richards JP, Ojha AK. 2012. Targeting drug tolerance in mycobacteria: a perspective from mycobacterial biofilms. Expert Rev Anti Infect Ther 10:1055–1066. https://doi.org/10.1586/eri.12.88.
54. Nikitushkin VD, Demina GR, Shleeva MO, Guryanova SV, Ruggiero A, Berisio R, Kaprelyants AS. 2015. A product of RpfB and RipA joint enzymatic action promotes the resuscitation of dormant mycobacteria. FEBS J 282:2500–2511. https://doi.org/10.1111/febs.13292.
55. Gordhan B, Parish T. 2001. Gene replacement using pre-treated DNA. Mol Med 54:77–92. https://doi.org/10.1385/1-59259-147-7:077.
56. Smith AM, Klugman KP. 1997. "Megaprimer" method of PCR-based

mutagenesis: the concentration of megaprimer is a critical factor. Biotechniques 22:438–442.
57. Snapper SB, Melton RE, Mustafa S, Kieser T, Jacobs WR, Jr. 1990. Isolation and characterization of efficient plasmid transformation mutants of *Mycobacterium smegmatis*. Mol Microbiol 4:1911–1919. https://doi.org/10.1111/j.1365-2958.1990.tb02040.x.
58. Parish T, Stoker N. 2000. Use of a flexible cassette method to generate a double unmarked *Mycobacterium tuberculosis tlyA plcABC* mutant by gene replacement. Microbiology 146:1969–1975. https://doi.org/10.1099/00221287-146-8-1969.
59. Stover CK, de la Cruz V, Fuerst TR, Burlein JE, Benson LA, Bennett LT, Bansal GP, Young JF, Lee MH, Hatful GF, Snapper SB, Barletta RG, Jacobs WR, Jr, Bloom BR. 1991. New use of BCG for recombinant vaccines. Nature 351:456–460. https://doi.org/10.1038/351456a0.